PAPER

Check for updates

Modulation of intramolecular Fe oxidation with distance and driving force in Ru–Fe photocatalysts†

Christian Herrero, [a] Frédéric Banse, [*a] Winfried Leibl [b] and Annamaria Quaranta [*b]

In this paper we have investigated the efficiency of the intramolecular electron transfer process in a family of Ru^{II}–Fe^{II} dyads, previously shown to perform the light-driven activation of an iron-bound water molecule. The Ru chromophore and Fe catalytic units are connected at different lengths through a triazole group attached to an alkyl chain containing either three or five carbon atoms. The driving force for Fe oxidation is modified by adding ethyl ester substituents on the bipyridines completing the coordination sphere of a $[Ru(bpy)_3]^{2+}$-like chromophore. Transient absorption measurements and simulations were used to obtain the rate constants of internal charge transfer for the different complexes. The parameters governing the electron transfer process, reorganisation energy λ and electronic coupling H_{AB} were obtained, and the observed variations are discussed within the framework of Marcus theory, which can help in understanding how to optimize the design of molecular photo-catalysts.

Introduction

The past decades have witnessed a tremendous development of efficient and selective light-driven catalytic processes, notably in the fields of synthetic photochemistry[1] and solar fuels.[2–5] When compared to electro- or thermo-catalytic procedures, a challenge inherent to photocatalysis is the synchronisation of the fast physical processes of photon absorption and generation of excited states (fs to ns timescale) with the slow chemical reactions involving multi-electron, multi-proton transfers and structural rearrangements necessary to perform catalysis. These two functions, light absorption and catalysis, can either be assumed by the same molecule, a 'photocatalyst', or by two distinct units: one capable of performing photo-induced redox processes (photoredox unit) activating a second catalytic unit for chemical transformations. Only a few catalysts behave as photocatalysts,[6–10] as the requirements associated with the absorption of visible light and generation of excited states well-suited to undergo redox reactions limit their scope.[11] Moreover, sustaining efficient light absorption throughout its

different redox states may interfere with the multi-electron catalytic processes. These limits can be overcome with the addition of an appropriate chromophore. In photocatalytic systems where the functions of light absorption and catalysis are assumed by different units, the initial step consists in generating efficiently, that is in high yield, a long-lived charge-separated (CS) state between the two moieties *via* photo-induced electron transfer (ET).

A family of complexes that well serves as a photoredox component is that of ruthenium polypyridines, widely used for their stability and tuneable properties.[12] These complexes are employed either in bimolecular configurations,[13,14] or in covalently linked chromophore–catalyst assemblies.[12,15] The latter approach offers the possibility to go beyond the diffusion-limited processes which characterise the bimolecular approach and, at the same time, allows optimising the structural elements that influence the formation of a CS state which, within the framework of Marcus theory,[16] is controlled by the driving force $(-\Delta G^0)$, the reorganisation energy (λ), and the electronic coupling (H_{AB}) between the two redox partners. In linked chromophore–catalyst systems, the electronic coupling depends on the nature of the donor and acceptor units as well as the bridge that connects those two moieties. Indeed, the bridge not only sets the distance between the donor and acceptor, but it also determines the electron transfer mechanism that operates between them, that is *via* tunnelling or hopping through the bridge.[17–19] The molecular orbitals of the

a Université Paris-Saclay, CNRS, Institut de Chimie Moléculaire et des Matériaux d'Orsay, 91400 Orsay, France. E-mail: frederic.banse@universite-paris-saclay.fr
b Université Paris-Saclay, CEA, CNRS, Institute for Integrative Biology of the Cell (I2BC), 91198 Gif-sur-Yvette, France. E-mail: annamaria.quaranta@cea.fr
† Electronic supplementary information (ESI) available. See DOI: https://doi.org/10.1039/d4nj02755h

bridge, if significantly higher in energy than those of the donor and acceptor, do not participate directly in the process, but these represent virtual states determining the electronic coupling, H_{AB}, between the two units: in this case, the electron transfer reaction proceeds *via* a super-exchange mechanism, and the ET rates exhibit an exponential dependence on the distance. On the other hand, if the molecular orbitals of the bridge involved in the electron transfer lie at similar energies as the donor and/or acceptor, the bridge participates directly in the electron transfer process which occurs *via* a hopping mechanism, less sensitive to the distance between the donor and the acceptor.[20,21]

In this work, we examine the impact of distance and driving force on the intramolecular electron transfer process in a family of covalently linked ruthenium chromophore–catalyst complexes. The aim is to evaluate the role of the intervening triazole-alkyl chain bridge, as well as the influence of the driving force, on the efficiency of the intramolecular ET, in an effort to go toward a mechanistically driven approach to photocatalysis. The complexes investigated, designed to perform the visible light activation of the catalytic unit,[22] are shown in Fig. 1. The chromophore units are bis-heteroleptic ruthenium complexes bearing either bipyridine ligands (**1** and **2**), or modified bipyridines featuring four electron-withdrawing ethyl ester units on their periphery (**3** and **4**) having different lengths between their components. The catalyst, $[\mathbf{Fe^{II}(L_5^2)Cl}]^+$, is an Fe^{II} ion wrapped by a penta-dentate amine/pyridine ligand (L_5^2) reported to perform the catalytic oxidation of organic substrates in the presence of oxygen-containing oxidants, and for which the spectroscopic signature of the active $Fe^{IV}(O)$ intermediate has been reported.[23,24] In a previous study involving **1-OH$_2$**, where the chloride ligand is substituted by a water molecule, we have shown that upon the absorption of visible light, the complex undergoes two sequential one-electron photo-oxidations of the iron catalyst leading to the formation of an active $Fe^{IV}(O)$ species, able to perform oxygen atom transfer onto a substrate.[22]

As mentioned above, the bridge connecting the Ru-chromophore and the Fe-based catalyst is a triazole unit, resulting from "click" synthetic procedures,[25] connected to a saturated alkyl chain containing either three (3C) or five (5C) –CH$_2$– units. Ruthenium chromophores are well-suited for click procedures,

with numerous examples being reported.[26–34] The role of the triazole bridge in photo-induced and thermal electron transfer processes has been investigated in the literature.[30,35] In the donor–acceptor systems examined, distinctive photo-induced electron transfer processes have been identified: hopping pathways resulting in fast charge separation;[36–38] tunnelling pathways in Zn-porphyrin–fullerene dyads;[39–41] but also cases where the photo-induced CS process was slow[42] or blocked[43,44] although thermodynamically feasible. An asymmetric role of the bridge with respect to photo-induced oxidation or reduction within the same system has also been reported.[36]

A successful method, to increase the driving force for the intramolecular electron transfer and stabilise it over time, is the flash-quench method which consists in quenching the excited state of the chromophore either by adding in excess amounts, or by grafting on it, an electron donor or acceptor, in order to generate either the reduced or oxidised state of the chromophore, respectively. This species is a better reductant (oxidant) than the excited state and is longer-lived because its disappearance relies on second-order charge recombination with the oxidised (reduced) quencher. Under such conditions (*i.e.* thermal electron transfer), electron transfer through the triazole bridge could be observed even when hindered in the excited state.[26,27,34,41,45–47]

Results and discussion

Electrochemical properties

Cyclic voltammetry studies have been performed on the reference catalyst compound $[\mathbf{Fe^{II}(L_5^2)Cl}]^+$ and on dyads to obtain the driving force for possible electron transfer processes occurring between the chromophore and the catalyst. For $[\mathbf{Fe^{II}(L_5^2)Cl}]^+$, the Fe^{III}/Fe^{II} redox event is observed at $E_{1/2} = 0.60$ V *vs.* SCE in acetonitrile.[22] Compounds **1** and **2** containing unmodified bipyridines on the chromophores present the same electrochemical profile (Fig. S1, ESI†): oxidation of Fe^{II} to Fe^{III} appears at 0.58 V, while the Ru^{III}/Ru^{II} redox process is observed at $E_{1/2} = 1.25$ V (1.24 V for **2**), allowing for a driving force $-\Delta G^0 = 0.66$ (0.67) eV for intramolecular Fe^{II} oxidation by Ru^{III}. For both compounds bearing ester bipyridine groups, **3** and **4**, Fe^{II} oxidation occurs at $E_{1/2} = 0.59$ V, while the Ru^{III}/Ru^{II} wave appears at $E_{1/2} = 1.45$ V, exhibiting a +0.20 V anodic shift as compared to the unmodified bipyridine analogues. This can be explained by the incorporation of four electron-withdrawing groups which induce a decrease in the electronic density at the metal centre. This results in an increased driving force ($-\Delta G^0 = 0.86$ eV) to perform Fe^{II} oxidation. Thus, we anticipate that the ester-containing dyads should be more efficient in generating the Fe^{III} species.

On the cathodic side, reduction waves are observed at -1.32 V *vs.* SCE for **1** and **2** and at -0.92 V for **3** and **4**, respectively. These processes, assigned to the reduction of a bipyridine of the ruthenium chromophore ($[Ru^{II}(bpy)_2(bpy)^{•-}]^+$), will be short-handed as Ru^I in the following text. The reduction

1 - X = H, n = 1
2 - X = H, n = 3
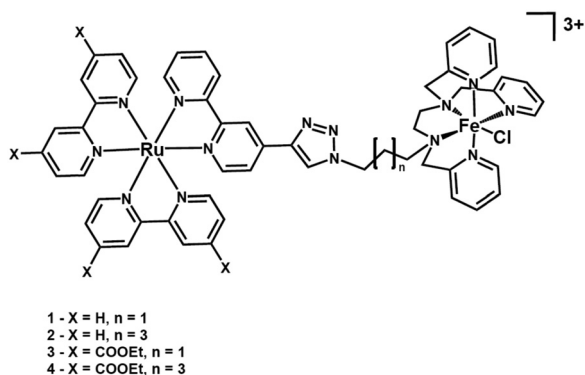**3** - X = COOEt, n = 1
4 - X = COOEt, n = 3

Fig. 1 Structure of the compounds studied.

Table 1 Summary of mid-point potentials for the different dyads in acetonitrile in the presence of 0.1 M of tetrabutyl-ammonium hexaflouro-phosphate (TBAPF$_6$), reported *vs.* SCE; ΔG for Fe oxidation has been obtained from $\Delta G^0 = F(E_{1/2}(Fe^{III}/Fe^{II}) - E_{1/2}(Ru^{III}/Ru^{II}))$, where F is the Faraday constant ($F = N_A e$).

Complex	$E_{1/2}(Fe^{III}/Fe^{II})$/V	$E_{1/2}(Ru^{III}/Ru^{II})$/V	ΔG^0/eV	$E_{1/2}(Ru^{II}/Ru^{I})$/V
1	0.58	1.25	−0.67	−1.32
2	0.58	1.24	−0.66	−1.32
3	0.59	1.45	−0.86	−0.92
4	0.59	1.45	−0.86	−0.92

potential of the ruthenium excited state (Ru*) for the process Ru* → Ru^I, given by

$$E_{1/2}(Ru^*/Ru^I) = E_{1/2}(Ru^{II}/Ru^I) - E^{00}(Ru^*)$$

with $E^{00}(Ru^*)$ estimated from the emission spectra of the chromophore,[48] amounts to 0.80 V *vs.* SCE for the dyads **1** and **2** and to 1.10 V for the ester modified dyads. These results suggest that Ru* should be able to oxidise Fe^{II} to Fe^{III} in all the dyads, with driving forces $-\Delta G^0 = -E_{1/2}(Fe^{III}/Fe^{II}) + E_{1/2}(Ru^*/Ru^I) = +0.22$ eV and $+0.52$ eV. As in previous studies,[26,27,46,47] no redox event associated with the triazole bridge was observed. This suggests that in these dyads, a super-exchange mechanism rather than electron-hopping through the bridge should operate. To resume, the electrochemical data, reported in Table 1, indicate that Fe^{II} oxidation is thermodynamically feasible from both Ru^{III} and Ru* species and that both electron transfer processes are more favoured in the ester-substituted complexes.

Photophysical properties

The absorption spectrum of the Fe^{II} redox state of the $[Fe^{II}(L_5{}^2)Cl]^+$ catalyst exhibits a maximum at 400 nm ($\varepsilon = 5000$ M^{-1} cm^{-1}), originating from an MLCT Fe^{II} → pyridine transition.[22] Upon excitation at 355 nm, an emission spectrum (Fig. 2) with a
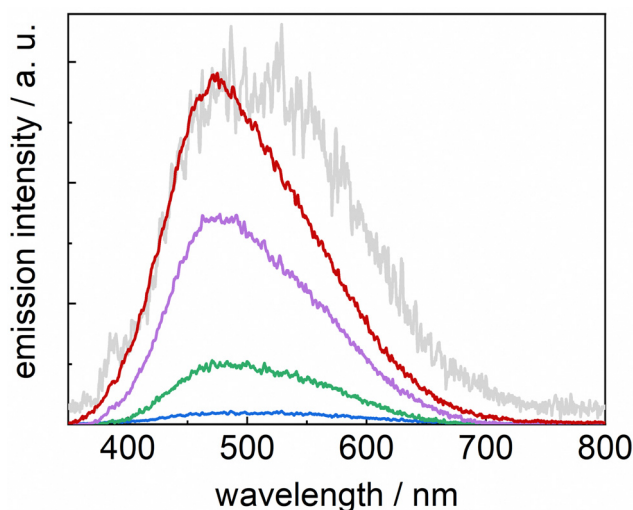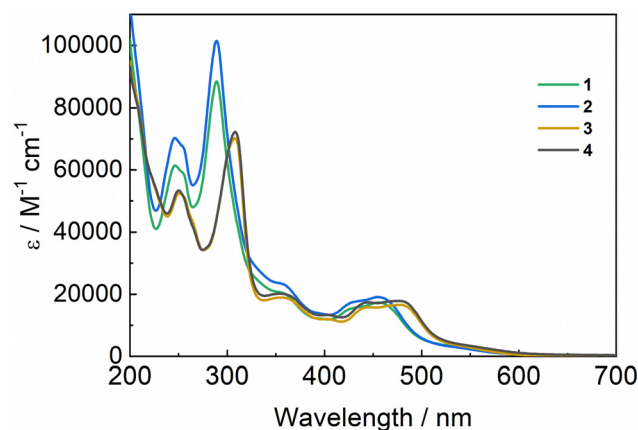
maximum at 475 nm is observed at early times (10 ns) which broadens at longer times (100 ns), hinting at the presence of a shoulder at ∼530 nm. This suggests the presence of heterogeneity in the excited states, some possibly close in energy to the chromophore's ones. No transient absorption was observed, even at short times (Fig. S2, ESI†). The decay kinetics of the observed emission could not be resolved as it disappears within the time resolution of our apparatus; however, from the spectra evolution, it could be estimated to be ∼30 ns. Such lifetime, uncommonly long for Fe^{II} polypyridine complexes, has previously been observed for similar iron complexes for which high-spin (HS) Fe^{II} excited states, lower in energy than ^{1}MLCT, are populated and deactivated *via* a transition to a low-spin (LS) state.[49,50] Equilibration between different HS states has been observed to cause biphasic decays.[50]

In the case of the chromophore–catalyst complexes, the absorption spectra (Fig. 3) exhibit a band at 290 nm (310 nm for the ester-bearing bipyridines), originating from the chromophore π–π* transition, and broad MLCT bands in the 400–500 nm region. In line with previously published results,[51,52] absorption bands for the ester-bipyridines complexes are red-shifted by ∼20 nm. Such a shift is reflected in the emission spectra (Fig. S3, ESI†) where maxima are observed at 610 nm for complexes **1** and **2**, and at 640 nm for **3** and **4**. This evidences, in agreement with the electrochemical results, the presence of a low-lying LUMO in the latter group. No emission bands associated with the catalyst were observed because excitation light at 460 nm is only absorbed by the ruthenium moiety ($\varepsilon[Fe^{II}(L_5{}^2)Cl]^+ < 1000$ M^{-1} cm^{-1}).

All the complexes studied exhibit biexponential emission decay kinetics (Fig. 4 and Table 2), sharing a long-living component ($\tau = 1100$ ns), slightly longer than that of the reference $[Ru(bpy)_3]^{2+}$.[48] This has previously been observed for ruthenium chromophores functionalised with the triazole attached *via* its carbon atom.[27,47] Biexponential decay of emission, often observed for heterobimetallic complexes,[51,53,54] may have several causes. It can be due to the presence of conformers with different efficiencies for quenching of the excited state by

Fig. 2 Evolution of the emission spectrum of the catalyst moiety in the H$_2$O/CH$_3$CN (4:1) mixture. Emission-gated spectra (gate: 10 ns) were obtained upon excitation with 355 nm laser flash (energy: 10 mJ) of an argon purged solution.

Fig. 3 Ground state absorption spectra for the complexes investigated in H$_2$O/CH$_3$CN (4:1).
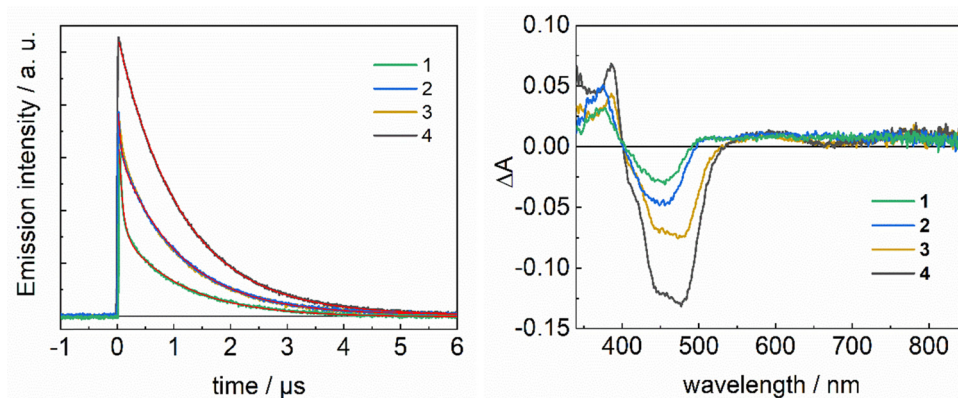
Fig. 4 Emission kinetics at the emission maximum (left) and transient absorption spectra at 100 ns (right) after the laser pulse, for the different compounds in H_2O/CH_3CN (4 : 1). Optically matched absorption at 460 nm. Decays have been fitted with a biexponential curve (red traces). On the right, the amplitude of the absorption spectra, taken at 100 ns after the laser pulse, is consistent with the excited state lifetimes.

Table 2 Emission maxima and emission lifetimes. Lifetimes have been obtained from the biexponential fit of emission decays (cf. ESI)

Complex	λ_{EM}/nm	τ_1/ns	τ_2/ns
$[Fe^{II}(L_5^2)Cl]^+$	470, 530	~ 30	> 30
1	610	1100 (39%)	70 (61%)
2	610	1100 (74%)	50 (26%)
3	650	1100 (81%)	120 (19%)
4	650	1150 (98%)	100 (2%)

energy/electron transfer, or from the equilibration between close-lying excited states. It is worth noting that in the compounds studied, the bridge might present some flexibility due to the alkyl chain,[55] allowing for different conformations, some possibly more prone to quenching. Regarding the possibility of having quenching by energy transfer, we notice that the relative amplitude of the fast emission phase is significantly lower for the ester-containing complexes, a fact that is tentatively attributed to the preferential localization of the electron on the ester-substituted bipyridine groups in the MLCT excited state (*Ru).[52,53] Such fast phase is largest for complex 1 where the shortest distance between the Fe atom and the excited state on the Ru chromophore is expected, in particular if the latter is localised on the bipyridine with the attached triazole linker. These observations are consistent with a possible energy transfer occurring in the conformers presenting a short-lived emission. However, the energy levels of the catalysts should lie higher than, or close to, those of the chromophore, a fact implying a slow energy transfer rate and inefficient quenching. Another possible explanation for the observed short-lived component could be a reductive quenching of *Ru^{II} state by Fe^{II}, which, as previously discussed, is an exergonic reaction. This process, which should be mediated by a hole-transfer super-exchange path between the acceptor LUMO and the HOMO bridge unit,[21] has often been observed in dyads bearing a triazole bridge.[35] Transient absorption spectra (Fig. 4) do not provide evidence for stable intermediates resulting from a photoinduced intramolecular reductive quenching of

*Ru^{II} by Fe^{II}. The absence of a detectable fraction of a Ru^{I} state absorbing at 510 nm[56] could, however, be explained with the recombination rate, for which $\Delta G^0 = -0.7$ eV, being faster than the CS rate, a scenario that prevents the observation of the transient CS state. With regard to driving force, the photoinduced reductive quenching of the ruthenium excited state should be favoured in ester-complexes 3 and 4 ($\Delta G^0 \sim -0.52$ eV), which, however, exhibit longer lifetimes. In consequence, the occurrence of reductive quenching as an explanation for the biphasic emission decay is considered as unlikely and we privilege the alternative explanation for the observed biexponential decay that is the equilibration between excited states close in energy. The ordering of the multiple MLCT excited states might be altered in dyads.[57] In particular, in agreement with the emission spectrum of $[Fe^{II}(L_5^2)Cl]^+$, the lower energy levels of the catalyst might be close to the higher MLCT levels of the chromophores, the more so for the unmodified-bipyridine.

To summarise, the photophysical studies have evidenced an heterogeneity of the excited states in these dyads with an excited state population having a short lifetime (~ 100 ns). This population is smaller in the presence of a long alkyl linker (5C) and for the ester-substituted groups on the ruthenium chromophore, both modifications resulting in locating the MLCT state away from the catalyst, which possibly reduces the interaction between the energy levels of the chromophore and the catalyst. Moreover, the collected results show that although the formation of a Ru^{I}–Fe^{III} CS state is thermodynamically accessible, it is not formed. Thus, we investigated the possibility to generate a long-lived Fe^{III} species using an external electron acceptor.

Photoinduced electron transfer in the presence of an external electron acceptor

We have previously observed[22] the intramolecular generation of Fe^{III} in complex 1, using $[Ru(NH_3)_5]^{2+}$, which is an optically transparent reversible electron acceptor.[58] We employ here methyl viologen (MV^{2+}) which is also able to oxidatively quench
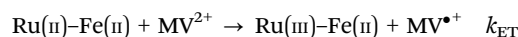
the chromophore $(E_{1/2}(MV^{2+}/MV^{\bullet+}) = -0.45$ *vs.* SCE)[59] in a bimolecular process creating a $MV^{\bullet+}$ radical and a Ru^{III} species which is then able to oxidise Fe^{II}. Reduction of MV^{2+} results in characteristic absorption bands at 400 nm ($\varepsilon = 41\,800$ M^{-1} cm^{-1}) and 605 nm ($\varepsilon = 13\,900$ M^{-1} cm^{-1}),[60] whereas conversion of Ru^{II} into Ru^{III} produces a depletion of absorption at 450 nm ($\Delta\varepsilon = -11\,300$ M^{-1} cm^{-1}).[61] The optical features of the $MV^{\bullet+}$ radical can thus be used to probe the efficiency of the initial bimolecular CS, to infer, using the kinetic evolution of the system, the subsequent steps, and to quantify the yields.

In the presence of 20 mM MV^{2+}, the emission of the excited state was quenched in all the compounds examined, although with different rates (k_{ET}) and yields. Interestingly, the quenching rate was smaller than diffusion-limited, varying from $k_{ET} \sim 10^7$ M^{-1} s^{-1} for the ester-containing complexes, to an order of magnitude higher with $k_{ET} \sim 3 \times 10^8$ M^{-1} s^{-1} for unmodified-bipyridine ones. This can be rationalised by the driving force values, which amounts to $-\Delta G^0 \sim 0.12$ eV and 0.42 eV, respectively. With ΔG^0 being certainly smaller than the reorganisation energy λ, the ET process is placed in the Marcus normal region. As such, the rate increases with $-\Delta G^0$ but it is smaller than the maximum rate (occurring at $-\Delta G^0 = \lambda$), which is, in the case of bimolecular reactions, limited by diffusion.

After the decay of the excited state, the presence of $MV^{\bullet+}$ is attested by the appearance of peaks at 400 and 605 nm

(Fig. S5, ESI†), while the bleaching at 450 (470, 480 for the esters) nm confirms the presence of the Ru^{III} species.

To investigate the light-induced internal ET events, we measured and analysed absorption transients at the wavelengths characteristic for Ru^{III} (450–480 nm) and the $MV^{\bullet+}$ radical (605 nm) (Fig. 5). In all cases, we found the decay of the Ru^{III} state to be faster than the decay of the reduced electron acceptor, evidencing that the reduction of Ru^{III} by Fe^{II} is competitive with back ET. To obtain the rate constants describing the dynamics of the system, we fitted the experimental data shown in Fig. 5, using the target model given below, which includes the initial bimolecular quenching by MV^{2+} (k_{ET}), both intramolecular (k_{IET}) and the final charge recombination between $MV^{\bullet+}$ and either Ru^{III} (k_{BET1}) or Fe^{III} (k_{BET2}).

$$Ru(II)–Fe(II) + MV^{2+} \rightarrow Ru(III)–Fe(II) + MV^{\bullet+} \quad k_{ET}$$

$$Ru(III)–Fe(II) \rightarrow Ru(II)–Fe(III) \quad k_{IET}$$

$$Ru(III)–Fe(II) + MV^{\bullet+} \rightarrow Ru(II)–Fe(II) + MV^{2+} \quad k_{BET1}$$

$$Ru(II)–Fe(III) + MV^{\bullet+} \rightarrow Ru(II)–Fe(II) + MV^{2+} \quad k_{BET2}$$

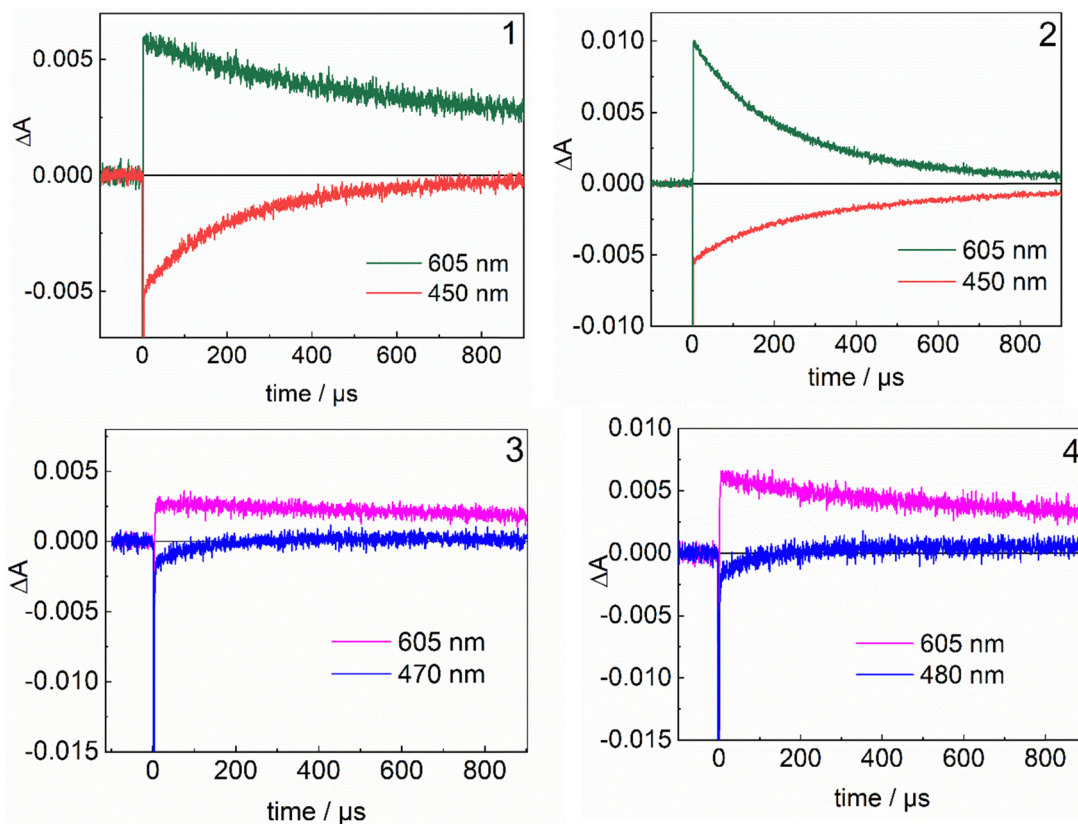The rate constant for the intramolecular oxidation of Fe^{II} is reported in Table 3 for the four complexes. The other

Fig. 5 Differential transient absorption kinetics at selected wavelengths in the presence of 20 mM MV^{2+} for the compounds studied in the H_2O/CH_3CN (4:1) argon-purged solution at 293 K. The solutions excited at 460 nm using a laser energy of $\sim$10 mJ and absorption at the excitation wavelength of 0.40.

parameters, as well as the species evolution resulting from simulations, are given in the ESI† (Fig. S6–S13). For complex **1**, 0.38 μM of Ru^{III} generated from the initial CS state evolves (k_{IET} = 3000 s^{-1}) into ∼0.21 μM of Fe^{III}. In the case of **2**, the longer lifetime of the excited state accounts for a higher yield of initial CS (0.62 μM), although the increased distance between the metals makes the intramolecular electron transfer slower (k_{IET} = 620 s^{-1}). For ester derivatives **3** and **4**, the oxidative quenching of the excited state by MV^{2+} results in a smaller concentration of the initial CS state, respectively 0.17 μM and 0.31 μM. Nevertheless, due to the increased oxidation potential of the Ru-chromophores with the ester-modified bipyridines, a higher k_{IET} (11 000 s^{-1}) is obtained, for intramolecular Fe^{III} generation in complex **3**. Finally, the longer metal-to-metal distance in **4** qualitatively explains the smaller rate constant compared to **3**. In an effort to rationalise the effect of driving force and distance on k_{IET}, the rate of the intramolecular electron transfer was measured at different temperatures for compounds **1**, **3** and **4** and the temperature dependence was analysed to obtain an estimation of the reorganisation energy λ and electron coupling H_{AB} for the different compounds (cf. ESI†). The values obtained (Fig. S14, ESI†) are reported in Table 3.

Among the complexes investigated, the fastest and most efficient intramolecular electron transfer was observed for complex **3**, which features a high oxidation potential of the Ru chromophore and the shorter Ru–Fe distance. The complex least efficient in generating Fe^{III} appears to be **2**, as the Ru^{III}/Ru^{II} redox potential is lower and the Ru–Fe distance is longer. These results could be rationalised within the framework of Marcus theory for ET. The reorganisation energy λ was found to be high (> 2 eV), explaining the rather slow intramolecular ET observed for all the dyads. Since for the prototypal chromophore $[Ru^{II}(bpy)_3]^{2+}$ no changes in the bonds occur upon reduction and λ is given only by the solvent contribution ($\lambda \sim 0.7$ eV),[62,63] we attribute the high reorganisation energy to significant changes in the bond lengths occurring on the Fe catalyst upon oxidation. This assignment is consistent with the spin state switch from high spin ($S = 2$) for $[Fe^{II}(L_5^2)Cl]^+$ and $[Fe^{II}(L_5^2)(OH_2)]^{2+}$ (ref. 64) to low spin ($S = 1/2$) for $[Fe^{III}(L_5^2)(OH)]^+$.[22] Such a spin state change in this family of complexes is accompanied by a Fe–N bond decrease of ca. 0.2 Å.[65] Although high, λ is quite similar among the different complexes, thus, it does not seem to be the reason for the differences observed among them. An increase of driving force, $-\Delta G^0$, by about 200 meV, due to the ester substitutions on the periphery of the Ru-chromophore, impacts instead the

activation energy E_A (cf. ESI†) and leads, as expected, to an increased rate k_{IET}, by a factor of ca. 3.5 and 13 for the short and long variants, respectively. Finally, the main parameter describing the distance dependence of the ET rate, the electronic coupling H_{AB}, was found to be strongly reduced (by at least a factor of 10, from ca. 0.20 meV to 0.07) by the introduction of two additional CH_2 groups in the linker.

Conclusions

From the results obtained, some conclusions can be drawn on the role of the bridge, as well as of the driving force, on both photoinduced energy and electron transfer processes in the chromophore–catalyst complexes. The observation of two excited state populations can be explained either by the presence of two conformers, due to some flexibility of the linker, or with the equilibration of the excited state between two close-lying energy levels. A photo-induced reductive quenching of the chromophore is thermodynamically favourable and it could explain the short-lived component for one of the conformers. However, this explanation seems unlikely considering that the ester-modified bipyridine complexes **3** and **4**, for which the driving force is considerably higher, exhibit the longest excited state lifetimes. Also, an energy transfer process seems improbable because the excited states of the catalyst lie higher in energy than that of the chromophore. We favour instead the presence of close-lying excited states that can equilibrate and this process is significantly reduced in the dyads with ester-modified bipyridines on the Ru-chromophore. Since the transient oxidation of Fe^{II} could not be observed via photo-induced intramolecular electron transfer, in order to generate the Fe^{III} species required to advance toward the active catalyst species, an external electron acceptor was added in the solution. In this case, the intramolecular oxidation of Fe^{II} to Fe^{III} was found to occur at different rates and with different yields depending on the driving force and the distance between the two metals. The triazole was not observed as an intermediate in the thermal intramolecular electron transfer process, consistent with the absence of a redox wave in the electrochemical measurements, confirming that the reaction takes place via tunnelling through the bridge. Among the parameters governing the electron transfer process, it was found that the reorganisation energy was very similar, while the electronic coupling H_{AB} was an order of magnitude smaller for the bigger metal–metal distances, making the intramolecular electron transfer considerably slower. Another parameter having a strong influence on the rate was found to be the driving force $-\Delta G^0$.

These results highlight the importance of the bridge and of ΔG^0 when designing complexes for photocatalysis. Optimising the efficiency of intramolecular electron transfer as described in this work is necessary for an efficient photodriven catalysis. However, for multi-electronic transformations, a further challenge consists also in optimising efficient charge accumulation on the catalyst. This requires similar characterisation of

Table 3 Parameters governing the rate constant for ET according to Marcus theory and rate constants for intramolecular ET at 293 K

Complex	ΔG^0/eV	λ/eV	H_{AB}/meV	k_{IET}/s^{-1}
1	−0.66	2.03	0.12	3100
2	−0.67	nd	nd	620
3	−0.86	2.39	0.25	11 000
4	−0.86	2.12	0.07	8300

photo-induced intramolecular ET to intermediate redox states of the catalyst, which might not only present different driving force and excited state quenching properties. More importantly, the bridge connecting the photosensitizer and the catalyst must be designed in a way to minimize deleterious charge annihilation due to fast ET from the photosensitizer excited state to the previously created oxidized catalyst species.[66,67] Extension of the mechanistic studies presented here using double-flash excitation procedures can help disentangle the reaction sequences operating for different redox states of the catalyst and these studies are currently ongoing in our lab.

Experimental

Chemicals were purchased from Acros and used without further purification. All solvents except for dichloromethane, acetonitrile and methanol were purchased from Aldrich or VWR and were used as received. Dichloromethane and acetonitrile were distilled over CaH_2, whereas methanol was distilled over Mg. NMR spectra were taken either on a Bruker AV 300 MHz or a Bruker 600 MHz spectrometer using the residual protonated solvent as an internal standard. Chemical shifts (δ) are given in parts per million (ppm) and coupling constants (J) are reported in hertz (Hz). Splitting patterns are designated as singlet (s), doublet (d), triplet (t), doublet of doublet (dd), and doublet of doublet of doublet (ddd). Splitting patterns that could not be interpreted or easily visualized are designated as multiplet (m). Electrospray mass spectra were recorded on a Thermo Scientific TSQ, or on a Bruker micrOTOFq mass spectrometer in the positive mode of detection (ESI$^+$).

Synthetic procedure

The synthetic procedure is shown in Fig. 6.

C3. N,N,N'-Tris(2-pyridylmethyl)-ethane-1,2-diamine (Trispicen) (471 mg, 1.41 mmol, 1 eq.) and toluene-4-sulfonic acid 3-azido-butane (1.60 g, 5.64 mmol, 4 eq.) were dissolved in 100 mL of acetonitrile. To this mixture were added K_2CO_3 (2.90 g, 21 mmol, 15 eq.) and KI (774 mg, 47 mmol, 0.30 eq.) and the reaction was stirred at 90 °C under an argon atmosphere for 72 hours. At this time the reaction mixture was allowed to cool to room temperature and filtered through a fritted filter in order to remove insoluble salts. The organic phase was removed under a reduced atmosphere and the resulting solid was chromatographed using neutral alumina and CH_2Cl_2: 1%MeOH as the eluent in order to collect the desired product (400 mg, 51% yield). ^{1}H NMR (300 MHz, CDCl$_3$) δ 8.47 (t, 3H, J = 5.6 Hz, Py-H); 7.59 (m, 3H, Py-H); 7.46 (d, 2H, J = 7.7 Hz, Py-H); 7.29 (d, 1H, J = 8.0 Hz, Py-H); 7.10 (m, 3H, Py-H); 4.36 (t, 2H, J = 7 Hz, CH_2-N$_3$); 3.80 (s, 4H, CH_2-Py); 3.68 (s, 2H, CH_2-Py); 2.69 (s, 4H, N-CH_2CH_2-N); 2.41 (t, 2H, J = 7.0 Hz, CH_2-N); 1.86 (m, 2H, CH$_2$-CH_2-CH$_2$-CH$_2$-CH$_2$-N$_3$); 1.46 (m, 2H, CH$_2$-CH$_2$-CH$_2$-CH_2-CH$_2$-N$_3$); 1.26 (m, 2H, CH$_2$-CH$_2$-CH_2-CH$_2$-CH$_2$). HRMS (ESI$^+$) [M + H]$^+$ = 445.2832. Calculated for $C_{25}H_{33}N_8$ = 445.2823.

E3. 4-Ethynyl-[2,2′]bipyridinyl (156 mg, 0.87 mmol, 1 eq.) and **C3** (386 mg, 0.87 mmol, 1 eq.) were dissolved in 20 mL (1 : 1 CH_2Cl_2/H_2O). The solution was purged and degassed 3 times with argon and vacuum. To this solution were added CuSO$_4$·5H$_2$O (326 mg, 1.30 mmol, 1.50 eq.) and sodium ascorbate
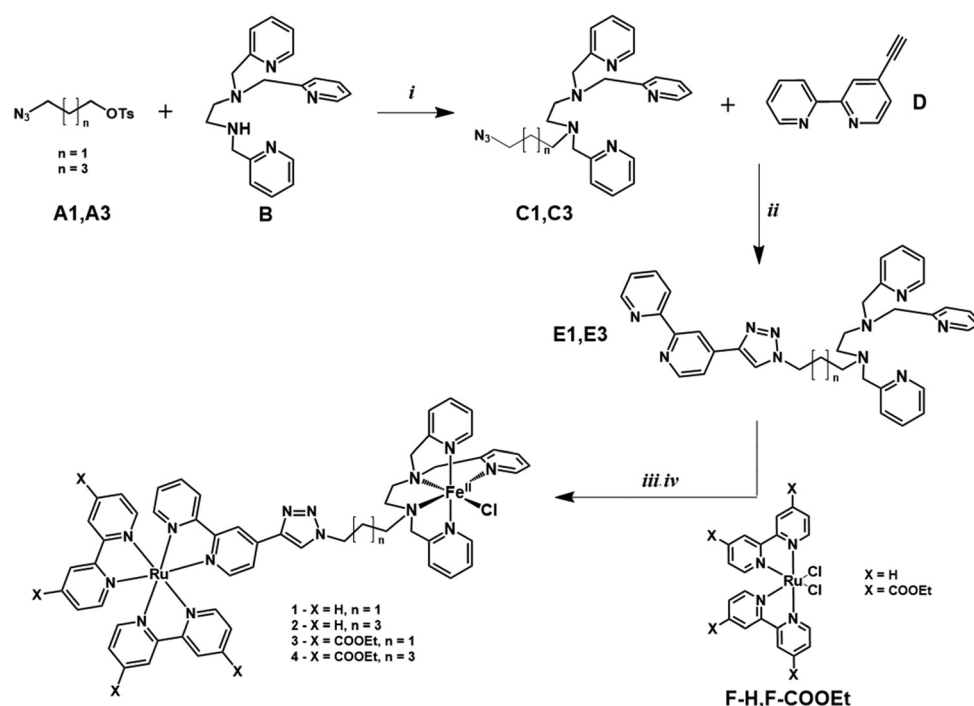
Fig. 6 Synthetic procedure for complex Ru–FeCl (**1-Cl**). (i) CH$_3$CN, K$_2$CO$_3$, 90 °C, 72 h (ii) CuSO$_4$·5H$_2$O, Na ascorbate, CH$_2$Cl$_2$:H$_2$O (iii) Ru(bpy)$_2$Cl$_2$, AgNO$_3$, MeOH, NaPF$_6$ (iv) FeCl$_2$ CH$_3$CN:MeOH. **C1**,[22] **D**,[27] **E1**, **F–H**,[51] **F-COOEt**[51] and **1** have been previously reported.

(522 mg, 2.61 mmol, 3 eq.). The mixture was allowed to react overnight under an argon atmosphere. At this time, the reaction mixture was transferred to a round bottom flask and 20 mL of a mixture containing 1.3 g of HEDTA and 0.6 g of NaOH was added, followed by mixing for one hour. The solution was extracted using CH_2Cl_2 and the product was purified via column chromatography (alumina. CH_2Cl_2 to CH_2Cl_2/2.5% MeOH) (227 mg, 41% yield). ^{1}H NMR (300 MHz, CDCl$_3$): δ 8.74 (d, 1H, J = 5.0 Hz, bpy-H); 8.68 (m, 2H, bpy-H); 8.49 (m, 4H, 3 Py-H, 1 bpy-H); 8.05 (s, 1H, tria-H); 7.95 (dd, 1H, J = 1.5, 5.0 Hz, bpy-H); 7.84 (td, 1H, J = 1.5, 7.8 Hz, bpy-H); 7.57 (m, 3H, pyr-H); 7.46 (d, J = 7.7 Hz, 2H, pyr-H); 7.34 (m, 2H, bpy-H); 7.30 (d, 1H, J = 5.5 Hz, Pyr-H); 7.11 (m, 3H, Py-H); 4.39 (t, 2H, J = 7.2 Hz, CH_2-Trz); 3.80 (s, 4H, CH_2-Pyr); 3.66 (s, 2H, CH_2-Pyr), 2.70 (s, 4H, CH_2-CH_2); 2.43 (t, 2H, J = 7.2 Hz, N-CH_2-CH$_2$-CH$_2$-CH$_2$-CH$_2$-Trz), 1.88 (q, 2H, J = 7.2 Hz, CH_2-CH$_2$-Trz); 1.49 (q, 2H, J = 7.2 Hz, CH_2-CH$_2$-CH$_2$-CH$_2$-Trz), 1.29 (q, 2H, J = 7.2 Hz, CH_2-CH$_2$-CH$_2$-Trz); HRMS(ESI$^+$) [M + H]$^+$ = 625.3520. Calculated for $C_{37}H_{41}N_{10}$ = 625.3510.

2-Ag. Ru(bpy)$_2$Cl$_2$ (75 mg, 0.155 mmol, 1 eq.) and AgNO$_3$ (52 mg, 0.31 mmol, 2 eq.) were dissolved in 5 mL of MeOH and stirred at room temperature for one hour. The resulting solution was filtered through filter paper into a round bottom flask containing compound **C3** (97 mg, 0.155 mmol, 1 eq.) and the resulting mixture was allowed to react under an argon atmosphere at 70 °C overnight. The solvent was evaporated under reduced pressure and the resulting solid was re-dissolved in a minimum amount of MeOH. The silver containing product **2** was precipitated by the dropwise addition of a saturated aqueous solution of NaPF$_6$ (190 mg, 85% yield).

^{1}H NMR (300 MHz, CD$_3$OCD$_3$): δ 8.99 (s broad, 2H, bpy-H); 8.95 (d, 1H, J = 8.1 Hz, bpy-H); 8.84 (d, 4H, J = 5.0 Hz, bpy-H); 8.55 (m, 3H, J = 8.0 Hz, Ru-Tz, Ru-bpy-H); 8.23 (m broad, 6H, bpy-H); 8.11 (q, 5H, J = 9 Hz, Trz-bpy-H, Ru-bpy-H); 7.91 (m, 4H Py-H); Ru-bpy, 7.59 (d, 5H, J = 8.0 Hz, bpy-H); 7.49 (broad, 4H, J = 7.6 Hz, bpy-H); 7.35 (7, 2H, Py-H); 4.35 (t, 2H, J = 7 Hz, CH_2-Trz); 4.03 (broad, 2H, CH_2-N); 3.79 (broad, 2H, CH_2-CH$_2$-N); 3.60 (s, 2H, N-CH$_2$-CH$_2$-N); 3.00 (broad, 2H, N-CH$_2$-CH$_2$-N); 2.91–2.84 (broad, 6H, CH$_2$-Pyr); 2.32 (dd, 2H, CH_2-CH$_2$-CH$_2$-Trz); 2.11 (m, 2H, CH_2-CH$_2$-Trz). HRMS (ESI$^+$) [M + H]$^{2+}$ = 645.1268. Calculated for $C_{57}H_{56}F_6N_{14}PRu$ = 645.1276.

2-Fe. (200 mg, 0.140 mmol, 1 eq.) was dissolved in 10 mL of CH$_3$CN and placed in a Schlenk tube which was degassed with argon. In a different Schlenk tube, FeCl$_2$·2H$_2$O (100 mg, 0.70 mmol, 5 eq.) was dissolved in 10 mL of MeOH and degassed with argon. The Fe-containing solution was transferred via cannula and the mixture was allowed to react overnight under an argon atmosphere. The content of the Schlenk tube was transferred to a round bottom flask where the solvents were removed under reduced pressure. The resulting solid was redissolved in a minimal amount of MeOH and the desired compound **3-Fe** was obtained as a red precipitate by the dropwise addition of a saturated aqueous solution of NaPF$_6$ (163 mg, 74% yield). HRMS(ESI$^+$) [M + PF$_6$]$^+$ = 637.1262. Calculated for $C_{57}H_{56}$ ClF$_6$FeN$_{14}$PRu = 637.1265.

3-Ag. F-COOEt (180 mg, 0.231 mmol, 1 eq.) and AgNO$_3$ (118 mg, 0.231 mmol, 3 eq.) were dissolved in 5 mL of MeOH and stirred at room temperature for one hour. The resulting solution was filtered through filter paper into a round bottom flask containing compound **A1** (138 mg, 0.231 mmol, 1 eq.) and the resulting mixture was allowed to react under an argon atmosphere at 70 °C overnight. The solvent was evaporated under reduced pressure and the resulting solid was redissolved in a minimum amount of MeOH. The silver containing product **3-Ag** was precipitated by the dropwise addition of a saturated aqueous solution of NaPF$_6$ (250 mg, 61% yield).

^{1}H NMR (300 MHz, CD$_3$OCD$_3$) δ: 9.05 (s, 1H, bpy-H); 8.95 (dd, 2H, J = 5 Hz, 1 Hz, Ester-bpy-H); 8.83 (d, 5H, J = 7 Hz); 8.71 (s, 1H, Trz-H); 8.62 (d, 1H, J = 5 Hz, bpy-H); 8.20 (m, 6H-Pyr-H); 8.08 (m, 5H, bpy-H); 7.94 (m, 2H, bpy-H); 7.70 (m, 3H, pyr-H); 7.61 (m, 5H, Pyr-H); 7.48 (dd, 1H, J = 5 Hz, 1 Hz, bpy-H); 4.59 (t, 2H, J = 7.0 Hz, Trz-CH_2-CH$_2$-CH$_2$-N); 4.48 (m, 10 H, J = 7 Hz, O-CH_2CH$_3$ and CH$_2$); 3.82 (t, 2H, J = 5 Hz, CH$_2$-Py); 3.62 (t, 2H, J = 5 Hz, CH$_2$-Py); 3.42 (q broad, 2 H, J = 8 Hz); 2.55 (q, 2H, J = 7 Hz, Trz-CH$_2$-CH_2-CH$_2$-N); 1.44 (t, 12H, J = 7 Hz, O-CH$_2$CH$_3$). HRMS(ESI$^+$) [M + PF$_6$]$^{3+}$ = 775.1537. Calculated for $C_{67}H_{68}$ AgF$_6$N$_{14}$O$_8$PRu = 775.1544.

3-Fe. 3-Ag (250 mg, 0.156 mmol, 1 eq.) was dissolved in 10 mL of CH$_3$CN and placed in a Schlenk tube which was degassed with argon. In a different Schlenk tube, FeCl$_2$·2H$_2$O (112 mg, 0.781 mmol, 5 eq.) was dissolved in 10 mL of MeOH and degassed with argon. The Fe-containing solution was transferred via cannula and the mixture was allowed to react overnight under an argon atmosphere. The content of the Schlenk tube was transferred to a round bottom flask where the solvents were removed under reduced pressure. The resulting solid was redissolved in a minimal amount of MeOH and the desired compound **3-Fe** was obtained as a red precipitate by the dropwise addition of a saturated aqueous solution of NaPF$_6$. (184 mg, 81% yield). HRMS(ESI$^+$) [M + 2PF$_6$–CH$_2$CH$_3$]$^+$ = 753.1431. Calculated for $C_{65}H_{65}$ ClF$_6$FeN$_{14}$O$_6$PRu = 753.1374.

4-Ag. F-COOEt (214 mg, 0.277 mmol, 1 eq.) and AgNO$_3$ (94 mg, 0.554 mmol, 2 eq.) were dissolved in 5 mL of MeOH and stirred at room temperature for one hour. The resulting solution was filtered through filter paper into a round bottom flask containing compound **A3** (173 mg, 0.277 mmol, 1 eq.) and the resulting mixture was allowed to react under an argon atmosphere at 70 °C overnight. The solvent was evaporated under reduced pressure and the resulting solid was redissolved in a minimum amount of MeOH. The silver containing product **4-Ag** was precipitated by the dropwise addition of a saturated aqueous solution of NaPF$_6$ (385 mg, 81% yield).

^{1}H NMR (300 MHz, CD$_3$OCD$_3$): δ 8.99 (m, 2H, Pyr-H); 8.83 (d, 5H, J = 8 Hz, Ester-bpy-H); 8.59 (s, 1H, Trz-H); 8.54 (s broad, 1H, bpy-H); 8.22 (t, 6H, H = 8 Hz, Ester bpy-H); 8.08 (q, 5H, J = 5 Hz, Ester-bpy-H); 7.87 (m, 3H, Pyr-H); 7.60 (broad, 4H, bpy-H); 7.48 (q, 4H, J = 8 Hz); 7.35 (q, 1H, J = 8 Hz, bpy-H); 4.48 (q, 8H, J = 7 Hz, O-CH_2CH$_3$); 4.34 (m, 2H); 4.06 (broad, 2H); 3.82 (broad, 2H); 3.61 (m, 2H); 2.83 (m, 8H, J = 7 Hz, 2 Hz, CH$_2$-Py); 2.33 (broad, 2 H); 1.44 (t, 12H, J = 8 Hz, O-CH$_2$-CH$_3$); HRMS(ESI$^+$) [M–CH$_3$CH$_2$ + PF$_6$]$^{3+}$ = 762.1382. Calculated for $C_{65}H_{64}$ AgF$_6$N$_{14}$O$_6$PRu = 762.1361.

4-Fe. 4-Ag (200 mg, 0.123 mmol, 1 eq.) was dissolved in 10 mL of CH$_3$CN and placed in a Schlenk tube which was degassed with

argon. In a different Schlenk tube, $FeCl_2 \cdot 2H_2O$ (89 mg, 0.615 mmol, 5 eq.) was dissolved in 10 mL of MeOH and degassed with argon. The Fe-containing solution was transferred *via* cannula and the mixture was allowed to react overnight under an argon atmosphere. The content of the Schlenk tube was transferred to a round bottom flask where the solvents were removed under reduced pressure. The resulting solid was redissolved in a minimal amount of MeOH and the desired compound **4-Fe** was obtained as a red precipitate by the dropwise addition of a saturated aqueous solution of $NaPF_6$. (184 mg, 81% yield). HRMS (ESI^+) $[M-2PF_6-CH_2CH_3]^{3+}$ = 463.1103. Calculated for $C_{67}H_{68}ClFeN_{14}O_{62}Ru$ = 463.114.

Electrochemistry. All electrochemical experiments were run under an argon atmosphere. Cyclic voltammetry measurements were recorded using an Autolab potentiostat controlled with a Nova 1.10 software package. The counter electrode used was a Pt wire and the working electrode was a glassy carbon disk carefully polished before each voltammogram with a 1 μm diamond paste, sonicated in an ethanol bath, and washed with ethanol. The reference electrode used was a SCE electrode isolated from the rest of the solution by a fritted bridge. The experiments were run with 1 mM solutions of complex in acetonitrile or acetone using 0.1 M tetrabutylammonium hexafluorophosphate as a supporting electrolyte.

Nanosecond laser flash photolysis. Transient absorption spectral and kinetic measurements were performed on an Edinburgh Instruments LP920 laser flash photolysis spectrometer system that incorporated a Continuum OPO for sample excitation (7 ns pulse duration). The OPO was pumped by a Continuum Surelite Q-switched Nd:YAG laser operating at 355 nm. The samples were excited by 460 nm wavelength pulses at ~10 mJ laser energy. The LP920 system uses a 450 W Xenon arc lamp as a source for the probe light for the transient absorption measurements. For kinetic measurements in the time range 10 ns to 100 μs, the Xenon arc lamp was pulsed. Detection is performed either *via* a Czerny–Turner blazed 500 nm monochromator (bandwidth: 1–5 nm) coupled with a Hamamatsu R928 photomultiplier tube (kinetic mode), or *via* a 500 nm blazed spectrograph (bandwidth: 5 nm) coupled with a watercooled ICCD nanosecond Andor DH720 camera (spectral mode). The samples, purged with argon for 10 minutes prior to each experiment, had an absorbance of ~0.40 at excitation wavelength. The presented transient absorption spectra were typically the average of 20–50 measurements. The kinetics profiles obtained in the presence of MV^{2+} were simulated using the free software QSoas program.[68] Values of known parameters such as the initial concentrations, $\Delta\varepsilon$, k_{ET} (obtained from the emission quenching experiments), were fixed and the fitting procedure was run using the ORDPACK engine.

Data availability

The data supporting this article have been included in the ESI.†

Conflicts of interest

The authors declare no conflict of interest.

Acknowledgements

References

1 L. Buzzetti, G. E. M. Crisenza and P. Melchiorre, *Angew. Chem., Int. Ed.*, 2019, **58**, 3730–3747.

2 L. Hammarström, *Acc. Chem. Res.*, 2015, **48**, 840–850.

3 T. Keijer, T. Bouwens, J. Hessels and J. N. H. Reek, *Chem. Sci.*, 2021, **12**, 50–70.

4 B. Zhang and L. Sun, *Chem. Soc. Rev.*, 2019, **48**, 2216–2264.

5 D. L. Ashford, M. K. Gish, A. K. Vannucci, M. K. Brennaman, J. L. Templeton, J. M. Papanikolas and T. J. Meyer, *Chem. Rev.*, 2015, **115**, 13006–13049.

6 J. Hawecker, J.-M. Lehn and R. Ziessel, *J. Chem. Soc., Chem. Commun.*, 1983, 536–538.

7 J. Grodkowski, T. Dhanasekaran, P. Neta, P. Hambright, B. S. Brunschwig, K. Shinozaki and E. Fujita, *J. Phys. Chem. A*, 2000, **104**, 11332–11339.

8 S. Funyu, T. Isobe, S. Takagi, D. A. Tryk and H. Inoue, *J. Am. Chem. Soc.*, 2003, **125**, 5734–5740.

9 S. Sato, T. Morikawa, T. Kajino and O. Ishitani, *Angew. Chem., Int. Ed.*, 2013, **52**, 988–992.

10 F. Kuttassery, S. Mathew, S. Sagawa, S. N. Remello, A. Thomas, D. Yamamoto, S. Onuki, Y. Nabetani, H. Tachibana and H. Inoue, *ChemSusChem*, 2017, **10**, 1909–1915.

11 A. Y. Chan, A. Ghosh, J. T. Yarranton, J. Twilton, J. Jin, D. M. Arias-Rotondo, H. A. Sakai, J. K. McCusker and D. W. C. MacMillan, *Science*, 2023, **382**, 191–197.

12 V. Balzani, P. Ceroni, A. Credi and M. Venturi, *Coord. Chem. Rev.*, 2021, **433**, 213758.

13 K. Zeitler, *Angew. Chem., Int. Ed.*, 2009, **48**, 9785–9789.

14 C. K. Prier, D. A. Rankic and D. W. C. MacMillan, *Chem. Rev.*, 2013, **113**, 5322–5363.

15 L. Sun, L. Hammarström, B. Åkermark and S. Styring, *Chem. Soc. Rev.*, 2001, **30**, 36–49.

16 R. A. Marcus and N. Sutin, *Biochim. Biophys. Acta, Rev. Bioenerg.*, 1985, **811**, 265–322.

17 G. J. Kavarnos and N. J. Turro, *Chem. Rev.*, 1986, **86**, 401–449.

18 O. S. Wenger, *Acc. Chem. Res.*, 2011, **44**, 25–35.

19 M. R. Wasielewski, *J. Org. Chem.*, 2006, **71**, 5051–5066.

20 A. Arrigo, A. Santoro, M. T. Indelli, M. Natali, F. Scandola and S. Campagna, *Phys. Chem. Chem. Phys.*, 2014, **16**, 818–826.

21 M. Natali, S. Campagna and F. Scandola, *Chem. Soc. Rev.*, 2014, **43**, 4005–4018.

22 C. Herrero, A. Quaranta, M. Sircoglou, K. Sénéchal-David, A. Baron, I. M. Marín, C. Buron, J.-P. Baltaze, W. Leibl, A. Aukauloo and F. Banse, *Chem. Sci.*, 2015, **6**, 2323–2327.

23 V. Balland, M.-F. Charlot, F. Banse, J.-J. Girerd, T. A. Mattioli, E. Bill, J.-F. Bartoli, P. Battioni and D. Mansuy, *Eur. J. Inorg. Chem.*, 2004, 301–308.

24 A. Bohn, C. Chinaux-Chaix, K. Cheaib, R. Guillot, C. Herrero, K. Sénéchal-David, J.-N. Rebilly and F. Banse, *Dalton Trans.*, 2019, **48**, 17045–17051.

25 H. C. Kolb, M. G. Finn and K. B. Sharpless, *Angew. Chem., Int. Ed.*, 2001, **40**, 2004–2021.

26 A. Baron, C. Herrero, A. Quaranta, M. F. Charlot, W. Leibl, B. Vauzeilles and A. Aukauloo, *Chem. Commun.*, 2011, **47**, 11011–11013.

27 A. Baron, C. Herrero, A. Quaranta, M.-F. Charlot, W. Leibl, B. Vauzeilles and A. Aukauloo, *Inorg. Chem.*, 2012, **51**, 5985–5987.

28 K. P. Chitre, E. Guillén, A. S. Yoon and E. Galoppini, *Eur. J. Inorg. Chem.*, 2012, 5461–5464.

29 C. Herrero, A. Quaranta, S. E. Ghachtouli, B. Vauzeilles, W. Leibl and A. Aukauloo, *Phys. Chem. Chem. Phys.*, 2014, **16**, 12067–12072.

30 N. Zabarska, A. Stumper and S. Rau, *Dalton Trans.*, 2016, **45**, 2338–2351.

31 S. Hohloch, D. Schweinfurth, M. G. Sommer, F. Weisser, N. Deibel, F. Ehret and B. Sarkar, *Dalton Trans.*, 2014, **43**, 4437–4450.

32 M. Braumüller, M. Staniszewska, J. Guthmuller and S. Rau, *Eur. J. Inorg. Chem.*, 2016, 4958–4963.

33 M. Ramachandran, S. Anandan and M. Ashokkumar, *New J. Chem.*, 2019, **43**, 9832–9842.

34 A. Charisiadis, E. Giannoudis, Z. Pournara, A. Kosma, V. Nikolaou, G. Charalambidis, V. Artero, M. Chavarot-Kerlidou and A. G. Coutsolelos, *Eur. J. Inorg. Chem.*, 2021, 1122–1129.

35 C. Müller, S. Bold, M. Chavarot-Kerlidou and B. Dietzek-Ivanšić, *Coord. Chem. Rev.*, 2022, **472**, 214764.

36 M. Natali, M. Ravaglia, F. Scandola, J. Boixel, Y. Pellegrin, E. Blart and F. Odobel, *J. Phys. Chem. C*, 2013, **117**, 19334–19345.

37 F. Zieschang, M. H. Schreck, A. Schmiedel, M. Holzapfel, J. H. Klein, C. Walter, B. Engels and C. Lambert, *J. Phys. Chem. C*, 2014, **118**, 27698–27714.

38 K. Yoosaf, J. Iehl, I. Nierengarten, M. Hmadeh, A.-M. Albrecht-Gary, J.-F. Nierengarten and N. Armaroli, *Chem. – Eur. J.*, 2014, **20**, 223–231.

39 G. de Miguel, M. Wielopolski, D. I. Schuster, M. A. Fazio, O. P. Lee, C. K. Haley, A. L. Ortiz, L. Echegoyen, T. Clark and D. M. Guldi, *J. Am. Chem. Soc.*, 2011, **133**, 13036–13054.

40 H. Imahori, K. Tamaki, D. M. Guldi, C. P. Luo, M. Fujitsuka, O. Ito, Y. Sakata and S. Fukuzumi, *J. Am. Chem. Soc.*, 2001, **123**, 2607–2617.

41 V. Nikolaou, F. Plass, A. Planchat, A. Charisiadis, G. Charalambidis, P. A. Angaridis, A. Kahnt, F. Odobel and

A. G. Coutsolelos, *Phys. Chem. Chem. Phys.*, 2018, **20**, 24477–24489.

42 A. Harriman, K. J. Elliott, M. A. H. Alamiry, L. Le Pleux, M. Severac, Y. Pellegrin, E. Blart, C. Fosse, C. Cannizzo, C. R. Mayer and F. Odobel, *J. Phys. Chem. C*, 2009, **113**, 5834–5842.

43 L. Zedler, P. Wintergerst, A. K. Mengele, C. Müller, C. Li, B. Dietzek-Ivanšić and S. Rau, *Nat. Commun.*, 2022, **13**, 2538.

44 S. Bold, T. Straistari, A. B. Muñoz-García, M. Pavone, V. Artero, M. Chavarot-Kerlidou and B. Dietzek, *Catalysts*, 2020, **10**, 1340.

45 P. Farras, S. Maji, J. Benet-Buchholz and A. Llobet, *Chem. – Eur. J.*, 2013, **19**, 7162–7172.

46 S. Sheth, A. Baron, C. Herrero, B. Vauzeilles, A. Aukauloo and W. Leibl, *Photochem. Photobiol. Sci.*, 2013, **12**, 1074–1078.

47 P. Gotico, T.-T. Tran, A. Baron, B. Vauzeilles, C. Lefumeux, M.-H. Ha-Thi, T. Pino, Z. Halime, A. Quaranta, W. Leibl and A. Aukauloo, *ChemPhotoChem*, 2021, **5**, 654–664.

48 A. Juris, V. Balzani, F. Barigelletti, S. Campagna, P. Belser and A. Vonzelewsky, *Coord. Chem. Rev.*, 1988, **84**, 85–277.

49 S. Schenker, P. C. Stein, J. A. Wolny, C. Brady, J. J. McGarvey, H. Toftlund and A. Hauser, *Inorg. Chem.*, 2001, **40**, 134–139.

50 A. Draksharapu, Q. Li, H. Logtenberg, T. A. van den Berg, A. Meetsma, J. S. Killeen, B. L. Feringa, R. Hage, G. Roelfes and W. R. Browne, *Inorg. Chem.*, 2012, **51**, 900–913.

51 C. Herrero, A. Quaranta, R.-A. Fallahpour, W. Leibl and A. Aukauloo, *J. Phys. Chem. C*, 2013, **117**, 9605–9612.

52 A. G. Tebo, S. Das, R. Farran, C. Herrero, A. Quaranta, R. Fallahpour, S. Protti, M.-F. Charlot, A. Aukauloo and W. Leibl, *C. R. Chim.*, 2017, **20**, 323–332.

53 M. L. A. Abrahamsson, H. B. Baudin, A. Tran, C. Philouze, K. E. Berg, M. K. Raymond-Johansson, L. Sun, B. Åkermark, S. Styring and L. Hammarström, *Inorg. Chem.*, 2002, **41**, 1534–1544.

54 A. Johansson, M. Abrahamsson, A. Magnuson, P. Huang, J. Mårtensson, S. Styring, L. Hammarström, L. Sun and B. Åkermark, *Inorg. Chem.*, 2003, **42**, 7502–7511.

55 V. Balzani, A. Juris, M. Venturi, S. Campagna and S. Serroni, *Chem. Rev.*, 1996, **96**, 759–834.

56 C. P. Anderson, D. J. Salmon, T. J. Meyer and R. C. Young, *J. Am. Chem. Soc.*, 1977, **99**, 1980–1982.

57 L. Flamigni, S. Encinas, F. Barigelletti, F. M. MacDonnell, K.-J. Kim, F. Puntoriero and S. Campagna, *Chem. Commun.*, 2000, 1185–1186.

58 J. R. Pladziewicz, J. A. Broomhead and H. Taube, *Inorg. Chem.*, 1973, **12**, 639–643.

59 J. C. Luong, L. Nadjo and M. S. Wrighton, *J. Am. Chem. Soc.*, 1978, **100**, 5790–5795.

60 T. Watanabe and K. Honda, *J. Phys. Chem.*, 1982, **86**, 2617–2619.

61 P. Mueller and K. Brettel, *Photochem. Photobiol. Sci.*, 2012, **11**, 632–636.

62 P. Siders and R. A. Marcus, *J. Am. Chem. Soc.*, 1981, **103**, 741–747.

63 E. J. Piechota and G. J. Meyer, *J. Chem. Educ.*, 2019, **96**, 2450–2466.

64 P. Mialane, A. Nivorojkine, G. Pratviel, L. Azéma, M. Slany, F. Godde, A. Simaan, F. Banse, T. Kargar-Grisel, G. Bouchoux, J. Sainton, O. Horner, J. Guilhem, L. Tchertanova, B. Meunier and J.-J. Girerd, *Inorg. Chem.*, 1999, **38**, 1085–1092.

65 N. Ségaud, J.-N. Rebilly, K. Sénéchal-David, R. Guillot, L. Billon, J.-P. Baltaze, J. Farjon, O. Reinaud and F. Banse, *Inorg. Chem.*, 2013, **52**, 691–700.

66 M.-H. Ha-Thi, V.-T. Pham, T. Pino, V. Maslova, A. Quaranta, C. Lefumeux, W. Leibl and A. Aukauloo, *Photochem. Photobiol. Sci.*, 2018, **17**, 903–909.

67 P. Gotico, A. DelVecchio, D. Audisio, A. Quaranta, Z. Halime, W. Leibl and A. Aukauloo, *ChemPhotoChem*, 2018, **2**, 715–719.

68 V. Fourmond, *Anal. Chem.*, 2016, **88**, 5050–5052.